Experimental-Based Unified Unsteady Nonlinear Aerodynamic Modeling For Two-Dimensional Airfoils

Conference Paper · June 2015

DOI: 10.2514/6.2015-3167

4 authors:

Mohamed Yehia Zakaria
Military Technical College
32 PUBLICATIONS **81** CITATIONS
SEE PROFILE

Haithem Taha
University of California, Irvine
64 PUBLICATIONS **373** CITATIONS
SEE PROFILE

Muhammad R. Hajj
Virginia Polytechnic Institute and State University
273 PUBLICATIONS **2,675** CITATIONS
SEE PROFILE

Ahmed A Hussein
Virginia Polytechnic Institute and State University
9 PUBLICATIONS **9** CITATIONS
SEE PROFILE

AIAA Aviation
22-26 June 2015, Dallas, TX
33rd AIAA Applied Aerodynamics Conference

Experimental-Based Unified Unsteady Nonlinear Aerodynamic Modeling For Two-Dimensional Airfoils

Mohamed Y. Zakaria * Haithem E. Taha † Muhammad R. Hajj ‡
and Ahmed A. Hussein§

Unsteady force measurements of a plunging airfoil at different frequencies and mean angles of attack are used to construct frequency response models. The obtained frequency response models are then used to determine the linearized flow dynamics around each mean angle of attack, where an optimization-based linear system identification is performed to minimize the error between the predicted and measured frequency responses. Converting these models to state space form and writing the entries of the matrices as polynomials in the mean angle of attack, a global, unified unsteady model is developed. The developed reduced order model, represented in a state space form, is suitable for characterizing the nonlinear dynamical characteristics of the flow and the associated dynamics and control of a flying object.

Nomenclature

b	Airfoil semi-chord ($c/2$)
C_L	Lift coefficient
e	Error between measured and optimized values
f	Frequency (Hz)
G	Response gain function
h_a	Plunging displacement (half stroke)
k	Reduced frequency $\pi fc/U_\infty$
ℓ	Wing span (m)
P	Non-dimensional Laplace variable
Re	Reynolds number
T	Time period
U_∞	Free stream velocity
α_o	Airfoil mean angle of attack
α_{eff}	Effective angle of attack
ω	Angular frequency,(rad/s)
τ	Non-dimensional time
ρ	Air density
QS	Quasi-steady
AOA	Angle of attack
LEV	Leading edge vortex
TEV	Trailing edge vortex

*PhD candidate, Engineering Mechanics Department, Virginia Tech, Blacksburg, VA, 24061, AIAA Student Member
†Assistant Professor, Aerospace and Mechanical Engineering, University of California Irvine, AIAA Fellow Member
‡Professor, Engineering Mechanics Department, VA, Professional AIAA Member
§PhD student, Engineering Mechanics Department, Virginia Tech, USA

I. Introduction

Efficient representation of the aerodynamic loads is an indispensable objective for flight dynamicists. For relatively-slow, small amplitude maneuvers at small angles of attack, the linear analysis using quasi-steady or even simple unsteady models (e.g. Theodorsen's or Wagner's) may be sufficient. However, the analysis of rapid, large amplitude maneuvers invokes the need to develop unsteady, nonlinear aerodynamic models. Although high-fidelity simulations can be used to obtain accurate estimates for the flow quantities, they are too inefficient to be used for flight dynamics and control purposes or even for studying the nonlinear dynamic characteristics of the flow field per se.

A number of ad-hoc models have been developed to capture specific phenomenon and/or lift mechanism (e.g., dynamic stall). Leishman and Beddoes[1] developed a semi-empirical unsteady aerodynamic model to analyze the dynamic stall behavior. Goman and Khrabrov[2] developed an unsteady aerodynamic model in the form of a first-order delay differential equation to account for the hysteresis associated with the cobra maneuver. On the other hand, experimental-based approaches could be the most convenient to develop reduced order models for such complex flows. Reisenthel[3] developed an unsteady aerodynamic model that is based on the nonlinear indicial theory (Volterra kernels) to analyze the flight mechanics associated with high angle of attack maneuvers. However, this latter type (experimental-based) of a model requires a priori determination of the nonlinear indicial functions. Hence, it cannot be applied directly without prior numerical and/or experimental work.

Because of the recent low Reynolds number applications associated with fast time-varying, high angle of attack flights (e.g., flapping flight), there has been a recent flurry in the mathematical modeling of the associated unsteady nonlinear aerodynamic characteristics. Brunton and Rowley[4] developed an experimentally-based extension to Theodorsen's model of the lift frequency response[5] to low Reynolds number regime. Several extensions to the classical potential flow approach (i.e., shedding of starting-like vortices, applying the unsteady Kutta condition at the sharp trailing edge, and using the Kelvin's law of zero total circulation) to account for unconventional lift mechanisms can be found in the open literature. Ansari et al.[6,7] extended the classical potential flow work of Von Karman and Sears[8] to include the leading edge vortex effect on flapping wings by shedding vorticity from both leading and trailing edges. Wang and Eldredge[9] proposed a remedy for the high computational cost associated with Ansari's model. Instead of shedding constant-strength point vortices at each time step from both leading and trailing edges, they shed variable-strength point vortices at larger time lapses. Taha et al.[10] extended the application of Duhamel's superposition principle, usually applied in linear unsteady aerodynamics, to account for unconventional lift mechanisms. They were able to account for the contribution of the leading edge vortex on flapping wings in an unsteady fashion. Yan et al.[11] developed a geometrically-exact potential flow model to account for geometric nonlinearities and non-planar wake effects. Ramesh et el.[12] used the first coefficient in the Fourier series expansion of the bound circulation distribution to serve as a criterion for predicting the onset of flow separation at the leading edge, and called it the Leading Edge Suction Parameter (LESP). They showed that there is a critical value of the LESP (depending on airfoil shape and Reynolds number), which determines whether the flow is attached or separated at the leading edge, irrespective of the motion kinematics.

A number of studies have focused on the wake structure to understand the flow dynamics and the associated lift augmentation and attenuation at various reduced frequencies for pitching, plunging and surging motions. Rival et. al[13] conducted force and velocity-field measurements to study the leading-edge vortex (LEV) growth and detachment for a plunging profile at Re = 10,000, reduced frequency of k = 0.25, and a Strouhal number of St = 0.16, for three different leading-edge geometries. The leading-edge shape has a direct effect on the shear layer feeding the LEV, and consequently to some extent the development of the LEV which, in turn, affects the flow structure. This effect influences the arrival time of the rear (LEV) stagnation point at the trailing edge yielding to detachment of the LEV. Gursul identified two mechanisms of lift enhancement during small amplitude oscillations of rigid plunging airfoils: deflected jets at high Strauhal numbers and convected LEVs at low Strauhal numbers. The deflected jets are produced from dipoles formed from pairing trailing edge vortices (clockwise and counter-clockwise). These dipoles are asymmetric in position and strength. Convected LEVs is an effective means of lift enhancement for post-stall angles of attack. The authors assert that this form of flow control is particularly effective at resonance between the plunge frequency and the natural shedding frequency and its harmonics.

An optimum range of Strouhal number over which the thrust efficiency and lift are enhanced between 0.25 and 0.35 was determined by many authors [14], [15], [16], [17], [18] and [19]. Panah et al.[20] showed experimentally that the LEV circulation is highly sensitive to the Strouhal number in the range $0.3 < St <$

0.5, concurrent with an accelerated roll-up of the leading-edge vortex. Choi et al.[18] investigated numerically the flow structure and mean fluctuating lift for surging and plunging airfoils at low Reynolds numbers. Based on their analysis of the wake structure, the authors found that, in surging, the fluctuating forces amplified when the augmented force contributed from the LEV was in phase with the quasi-steady component then constructively increase the total fluctuating lift, and/or suppressed when it is out of phase where the two components cancels each other (destructively). Also, they determined that the same behavior was achieved for both surging and plunging motions, where the lock-in region occurred near the vortex shedding frequency.

From the above discussion, there is no analytical unsteady nonlinear aerodynamic model that can be used directly to characterize the local and global nonlinear dynamic characteristics of the airflow and, consequently, be used in the analysis of the dynamics and control of flying objects. The objective of this work is to develop linear dynamic models at different angles of attack for two dimensional airfoils from frequency response measurements. Then, these linearized models are unified to construct a global nonlinear unsteady aerodynamic model. The frequency response models are easily converted to the corresponding linear state space models with the quasi-steady lift coefficient used as the aerodynamic input, similar to the work of Taha et al.[10] Relating the state space models is then performed by expanding the entries of the model matrices into quadratic terms in the mean angle of attack.

II. Experimental Setup

The experiments were conducted in an open-jet-return low-speed wind tunnel blower type. The used airfoil is the NACA 0012 profile with chord length c = 0.14 m. The model spanned the entire width of the test section 0.63 m. A semi programmable control system was developed to record analog data from load balance and accelerometers. Experiments were conducted at Re = 79,900 and sinusoidal plunging motions were performed with a plunge amplitude of $h_o = 0.137c$ and reduced frequencies that varied from $k = 0.1$ to $k = 0.95$, respectively. Table 1 summaries the operating conditions of the performed experiments.

Table 1. Operating conditions for the conducted pure plunging experiment.

α_0	k	h_o (m)	c (m)	ℓ (m)
$0^o \leq \alpha_0 \leq 65^o$	$0.1 \leq k \leq 0.9$	0.0193	0.14	0.63

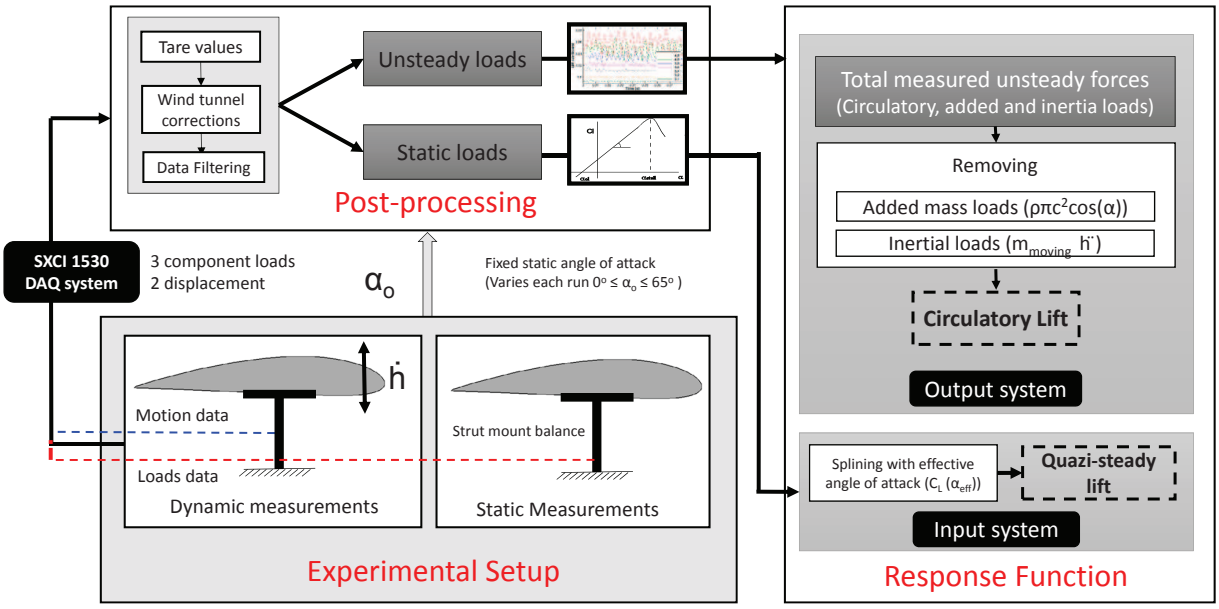

Figure 1. System identification process.

The system identification process to obtain the lift frequency response function is schematically presented in Figure 1. The process starts with the experimental setup block, which is composed of a plunging mechanism that is capable of performing static measurements over a wide range of angles of attack and also rigid enough to perform pure plunging motion at various frequencies. The output from this block is the force data sensed from the load balance (red dashed line) and the acceleration data coming from the accelerometers (blue dotted line). The second block is concerned with post-processing of the collected data. Due to the presence of experimental noise, a fourth-order, low pass butter-worth digital filter was used as a smoothing algorithm. Also, to avoid any phase shift due to filtration, zero-phase forward and reverse digital filtering is used.[21] In this process, the tare values were subtracted from the measurements, the tunnel corrections were applied, and finally the data were filtered. The third block describes how the lift response function is constructed. It is composed of two sub-blocks for the input and output data of the sought frequency response. In the first sub-block, the output data (circulatory lift coefficient) is determined by subtracting the inertial loads and added mass effects from the total measured unsteady loads. In the second sub-block, the quasi-steady lift coefficient (input) is computed based on the measured static lift curve and the measured plunging motion of the airfoil. The lift frequency response function is then obtained at each mean angle of attack α_o. The detailed experimental procedures can be found in a related previous work by zakaria et al.[22] The plunge motion is given by:

$$h(t) = h_a \sin 2\pi f t \tag{1}$$

and the effective angle of attack is defined as:

$$\alpha_{eff}(t) = \alpha_o + \frac{\dot{h}}{U_\infty} = \alpha_o + k\overline{H}\cos(2\pi f t) \tag{2}$$

where k is the reduced frequency, and $\overline{H}$ is the half-chord-normalized plunging amplitude. As such, the quasi-steady lift coefficients is determined from the effective angle of attack using the static lift measurements for NACA 0012 based on zakaria et al.[22] That is,

$$C_{Ls}(t) = \mathcal{C}_\mathcal{L}(\alpha_{\text{eff}}(t)) \tag{3}$$

where $\mathcal{C}_\mathcal{L}(\alpha)$ is the variation of the steady lift coefficient with the angle of attack. The circulatory loads represent the intrinsic part responsible for constructing the lift frequency response function. Therefore, extraction of such a component from the total lift measurement should be performed. The total force measurements include inertial, added mass, and circulatory contributions. As such, we write:

$$C_{L_{\text{circulatory}}}(t) = \left[L_{\text{measured}}(t) + (m_{\text{moving}} + m_{\text{added}})\ddot{h}(t)\right] / \left[\frac{1}{2}\rho U_\infty^2 c\right] \tag{4}$$

where $\ddot{h}(t)$ is the plunging acceleration, m_{moving} is the moving mass (wing profile and oscillatory rod), and m_{added} is the added mass. We adopt the geometrically-exact model of Yan et al.[11] for the added mass effects, then for our case we can write the added mass as:

$$m_{\text{added}} = \pi\rho b^2 \cos^2\alpha\ell$$

As such, the circulatory lift is obtained as

$$C_{L_{\text{circulatory}}}(t) = \left[L_{\text{measured}}(t) + (m_{\text{moving}} + \pi\rho b^2\cos^2\alpha\ell)\ddot{h}(t)\right] / \left[\frac{1}{2}\rho U_\infty^2 c\right] \tag{5}$$

III. Lift frequency response results

For each combination of α_o and k, the magnitude of the frequency response function G is obtained as:

$$|G| = \frac{|C_{L_{\text{circulatory}}}|}{|C_{Ls}|} \tag{6}$$

where $|.|$ is used to designate the amplitude of the signal. At each value of the mean angle of attack, the experiment is performed at various reduced frequencies to determine the variation of the magnitude $|G|$ with

the plunging frequency and, hence, construct the frequency response function for each angle of attack. These response functions are determined for 14 cases ($0 \leq \alpha_o \leq 65°$) with a reduced frequency range between 0.1 and 0.9.

Based on the results of the frequency response presented by zakaria et al.,[22] the flow dynamics was classified to three regimes. The first regime is the linear regime ($0^o \leq \alpha_o \leq 10$) before stall occurs. The stall regime bounds the occurrence of the stall and is characterized by the development and interactions of leading and trailing edge vortices ($15^o \leq \alpha_o \leq 40$). In addition, this regime is characterized by a change in the behavior of the flow dynamics from first order to second order by having a sharp jump in the response lift function attributed to the formation of the leading edge vortex. The third regime is a post stall regime ($45^o \leq \alpha_o \leq 65$), where the response function re-assumes its first-order dynamical behavior as observed in the linear regime with an attenuated response (i.e., lower values in comparison to Theodorsen's).

IV. Optimization based system identification

A. Optimization problem formulation

We seek a finite-dimensional approximation to a dynamical system that is infinitely dimensional even in its most simplified representation (two-dimensional, potential flow). The order of the sought finite-dimensional approximation is arbitrary. In fact, there is no consensus about the appropriate order of a finite-dimensional approximation even to the linear dynamical response (Theodorsen's and Wagner's). One can find useful second order approximation[23] and eighth-order approximation[24] to Wagner's response. For our purposes, we start with the regime of the most dynamically-rich response (i.e., the stall regime). By performing different levels of approximations, we find that the minimum order of a finite dimensional approximation that can satisfactorily fit the obtained data is four. As such, we write the gain as a transfer function of a fourth-order system, i.e.

$$G(p) = \frac{C_{L_{\text{circulatory}}}(p)}{C_{L_s}(p)} = \frac{b_3p^3 + b_2p^2 + b_1p + b_0}{p^4 + a_3p^3 + a_2p^2 + a_1p + a_0} \tag{7}$$

where, p is the non-dimensional Laplace variable corresponding to the non-dimensional time-variable $\tau = \frac{U_\infty t}{b}$. To obtain the magnitude of the frequency response of this transfer function, we substitute $p = ik$, which yields

$$|G(k)| = \sqrt{\frac{(b_0 - b_2\omega^2)^2 + (b_1\omega - b_3\omega^3)^2}{(a_0 - a_2\omega^2 + \omega^4)^2 + (a_1\omega - a_3\omega^3)^2}} \tag{8}$$

To determine the coefficients of the transfer function given in eq.7, we set up and solve, for each α_o, the optimization problem.

$$\min_{\boldsymbol{x}} \quad e^2_{|G|} = \sum_i^N \left(|G(k_i)| - |G_{\text{meas}}(k_i)|\right)^2 \quad \text{subject to}$$

$$\frac{b_0}{a_0} = 1 \;\text{ and }\; \mathcal{R}\left[\text{roots}(p^4 + a_3p^3 + a_2p^2 + a_1p + a_0)\right] < 0$$

where $\boldsymbol{x}$ represents the vector of design variables ($x = [a_0, a_1, a_2, a_3, b_0, b_1, b_2, b_3]$), $|G_{\text{meas}}(k_i)|$ is the measured frequency response at the data point k_i, N is the number of measurements, and $\mathcal{R}$ represents the real part of its argument. The first (equality) constraint has to do with the physical unity dc gain; that is, the ratio between the unsteady and steady loads at zero frequency must be unity. The second (inequality) constraint is to ensure that the selected transfer function given in eq.7 has poles with a negative real part; that is, we have stable flow dynamics.[25] We use sequential quadratic programming to solve the above posed optimization problem.

B. Linear Regime Regression

Figure 2 shows the calculated magnitude of the frequency response from the measured values at 0^o, 5^o and 10^o angles of attack. Additionally, we show plots of the gain functions as derived from Theodorsen's model and a fitted fourth-order system as shown in eq.7. The data and plots show that the measured values follow closely the predicted value with the simple-lag-type (first order) dynamic response of Theodorsen's function.

Since no considerable variations due to α_o were observed in this regime, we show a representative model for all experimental data in Fig. 3. The results show that Theodorsen's model, as well as the proposed model, capture the dynamical behavior of the measured frequency response in this regime.

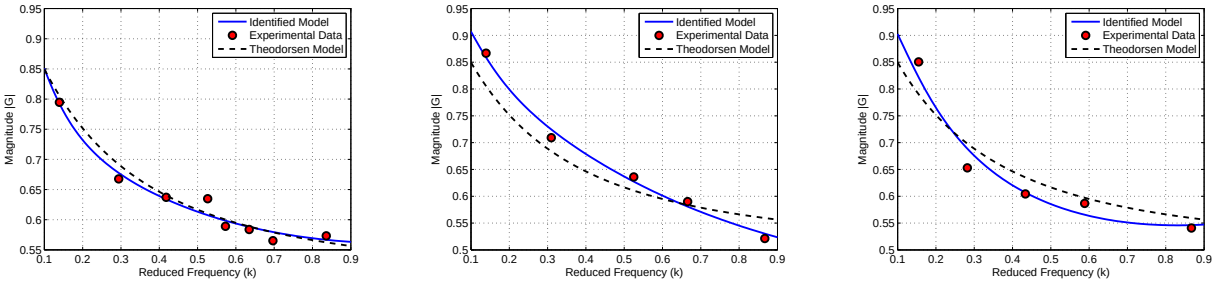

(a) 0^o AOA. (b) 5^o AOA. (c) 10^o AOA.

Figure 2. lift frequency response function for 0^o, 5^o and 10^o angles of attack

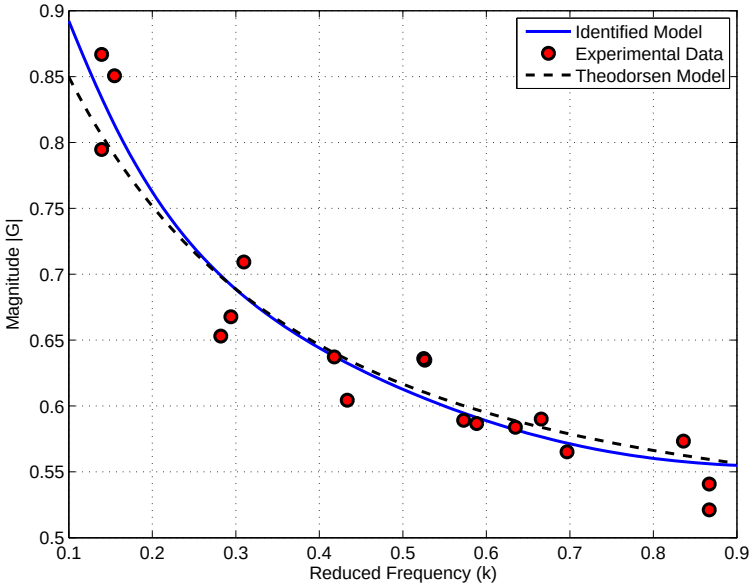

Figure 3. Lift frequency response function for linear regime (0^o - 10^o AOA)

Theodorsen's model is based on a linear approximation for the flow dynamics, which results in a frequency response that is independent of the operating condition and/or the amplitude of the aerodynamic input (airfoil motion). However, the geometric and non-planar-wake nonlinearities are expected to result in a different frequency response (i.e., linearized flow dynamics) at different operating conditions (angles of attack). Table2 summarizes the coefficients of the transfer function for each angle of attack and for the whole optimized regime.

Table 2. Optimal coefficient for fourth order transfer function for linear regime

α_0	$a_o = b_o$	a_1	a_2	a_3	b_1	b_2	b_3
0°	0.4526	4.5878	5.9066	2.8328	-2.5448	0.3615	0.0622
5°	2.2533	18.6981	24.3527	2.6800	-9.7925	-4.9991	1.6622
10°	0.8266	5.3246	4.8048	3.0480	-1.9627	-0.6053	-0.4887
$C_{Linear}(k)$	49.8945	426.2164	630.8317	456.1217	-284.7016	371.4162	-275.0544

C. Stall regime regression

In the stall regime, the frequency response is of particular importance because it cannot be predicted by Theodorsen's model. Even the model of Yan et al.,[11] though is geometrically valid for high angles of attack, it did not account for the leading edge vortex, which is an important contributor to the lift function in this regime. Figure 4 show the data points, as determined from the measurements of frequency response magnitudes for $\alpha_0 = 15^o$, 20^o, 25^o, 30^o, 35^o and 40^o. The response functions calculated from Theodorsen and the optimized response based on the fourth-order transfer function are also plotted in the same figures. As expected, the obtained frequency responses in this regime is quite different from Theodorsen's; both qualitatively and quantitatively. Unlike the monotonically decreasing behavior of Theodorsen's frequency response, which is a typical behavior for a simple lag (first-order) system, we note the decrease in the magnitude of the frequency response as the reduced frequency is increased up to a value near 0.65 - 0.7. Near that value, we observe a sharp increase in the magnitude of the frequency response. This is followed by a reduction in the value of the magnitude as the reduced frequency increased to around 0.9. The results show that, the proposed model was able to capture the flow dynamics based on the fourth order transfer function given in eq.7 for the stall regime. Table3 represents the optimal values for the proposed model coefficients.

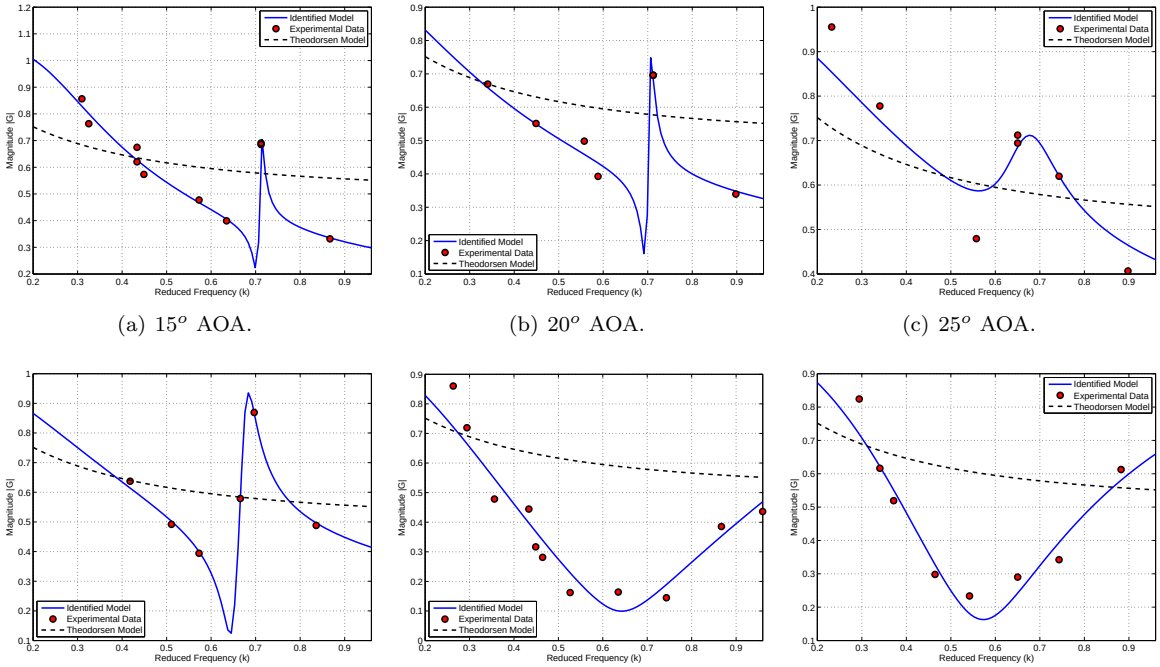

(a) 15^o AOA. (b) 20^o AOA. (c) 25^o AOA.

(d) 30^o AOA. (e) 35^o AOA. (f) 40^o AOA.

Figure 4. Lift response function for stall regime (α_o=15^o - 40^o).

The observed frequency response is an indication of a second-order dynamical nature of the system dynamics. This finding is quite important for unsteady engineering applications (e.g., flapping flight and wind turbines) as it suggests a lift-optimal frequency range around $k = 0.7$. It should be noted that the recent computational results of Choi and Colonius[18] showed a lift increase at $k = 0.7$, which is in agreement with the current findings. Moreover, the corresponding Strouhal number is 0.29, which is in agreement with the optimum frequency range found by Wang.[26] Furthermore, the identified model based on the experimental data for 35^o and 40^o models the second order response with increasing the reduced frequency to reach higher values.

Table 3. Optimal coefficient for fourth order transfer function for stall regime

α_0	$a_o = b_o$	a_1	a_2	a_3	b_1	b_2	b_3
15°	0.0340	0.2064	0.5766	0.4172	-0.1377	0.0711	-0.2763
20°	3.4364	11.6988	7.7076	23.4391	-0.9323	7.0927	-2.0411
25°	4.4385	10.8699	14.7049	28.5263	0.9014	13.2223	0.4271
30°	4.4173	12.7872	11.2184	27.4305	-0.0013	10.6354	-0.4121
35°	7.3720	23.4848	19.1630	3.4687	1.3809	16.8115	8.3945
40°	2.5492	7.5881	13.7106	6.4501	-0.7422	8.2961	1.6030

D. Post-stall regime regression

Figure 5 show Theodorsen gain lift function compared with experimental data and the identified model for angles of attack $\alpha_o = 45^o$, 50^o, 55^o, 60^o and 65^o. The results show similar characteristics to the response functions obtained in the linear regime. The difference is that, the response lift function has a smaller amplitude than its linear counterpart. Figure 5(f) shows the optimized identified model for the whole regime. It is clear from the figures that, each identified model per each angle of attack, has almost the same trend for the other (first order). Consequently, we can assume that the developed identified model presented in fig.5(f) adequately represents a good finite dimension approximation to the flow dynamics in this regime. Table4 represents the optimal values for the proposed model coefficients for the post stall regime.

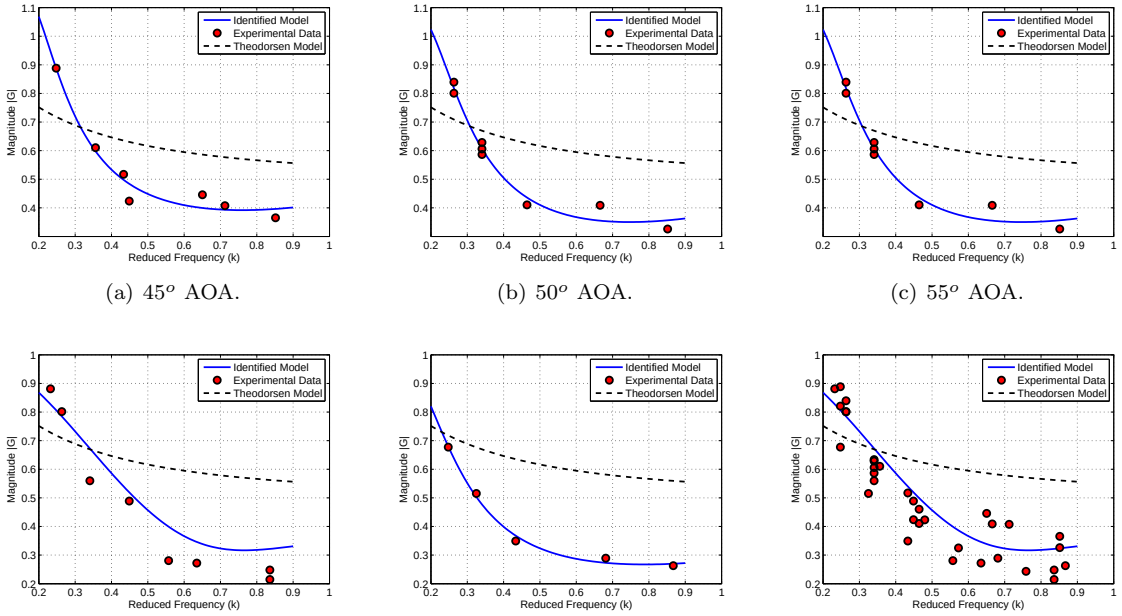

(a) 45^o AOA. (b) 50^o AOA. (c) 55^o AOA.

(d) 60^o AOA. (e) 65^o AOA. (f) 40^o - 65^o AOA.

Figure 5. Lift response function for post-stall regime (α_o=45^o - 65^o).

Table 4. Optimal coefficient for fourth order transfer function for post-stall regime

α_0	$a_o = b_o$	a_1	a_2	a_3	b_1	b_2	b_3
45°	0.2087	1.1791	5.0833	1.5380	-0.8888	1.3741	0.1572
50°	0.2453	1.4435	9.1347	0.1782	1.7240	2.8484	0.8080
55°	9.6511	33.2417	13.5051	20.5885	-4.1939	11.4316	2.4681
60°	20.4325	121.5241	423.4162	19.4391	83.9206	103.6480	8.8308
65°	0.4814	3.0270	9.0733	2.6695	-1.4444	2.3594	-0.5157
$C_{Post\ Stall}(k)$	0.1646	2.4162	22.7104	0.1249	-4.7538	6.3940	-5.1367

V. State space representation

Next we develop an efficient mathematical model that captures the unsteady aerodynamic behavior of a two-dimensional airfoil (henceforth referred to as the aerodynamic system). Since the state space formulation (a finite number of first-order differential equations) is the most convenient form for dynamics analysis, it is set to be the sought form for the developed model. The aerodynamic system uses the angle of attack or quasi-steady lift as inputs and yields the corresponding unsteady circulatory lift as an output.

A. State space modeling procedures

Having determined the optimized coefficients of the transfer function give by eq.8, we write the following corresponding state space model

$$\frac{d}{dt}\begin{pmatrix} X_1 \\ X_2 \\ X_3 \\ X_4 \end{pmatrix} = \begin{bmatrix} 0 & 1 & 0 & 0 \\ 0 & 0 & 1 & 0 \\ 0 & 0 & 0 & 1 \\ -a_4 & -a_3 & -a_2 & -a_1 \end{bmatrix} \begin{pmatrix} X_1 \\ X_2 \\ X_3 \\ X_4 \end{pmatrix} + \begin{pmatrix} 0 \\ 0 \\ 0 \\ 1 \end{pmatrix} C_{Ls} \tag{9}$$

$$\mathcal{Y} = \begin{bmatrix} b_o & b_1 & b_2 & b_3 \end{bmatrix} \begin{pmatrix} X_1 \\ X_2 \\ X_3 \\ X_4 \end{pmatrix} \tag{10}$$

where X is the vector of internal aerodynamic states, $\mathcal{U} = C_{L_s}$ is the aerodynamic input, taken here to be the quasi-steady lift coefficient, and $\mathcal{Y} = C_{L_{\text{circulatory}}}$ is the aerodynamic output, taken here to be the circulatory lift coefficient.

VI. Unified State Space Modeling

As shown in the previous section, the constructed models in the linear and post-stall regimes do not have a considerable dependence on the operating angle of attach and, as such, are combined in a single response function, each. On the other hand, the frequency response in the stall regime depends on α_o; the frequency and amplitude of the lift peak is different for various operating angles of attack. Since the constructed state space model is of the abstract form:

$$\begin{aligned} \dot{\boldsymbol{x}} &= [\boldsymbol{A}]\boldsymbol{x} + [\boldsymbol{B}]C_{L_s} \\ C_{L_{\text{circulatory}}} &= [\boldsymbol{C}]\boldsymbol{x} \end{aligned} \tag{11}$$

We propose combining the obtained linearized dynamics in the stall regimes at various angles of attack by writing the coefficients of the transfer function (consequently, the entries of the matrices) as polynomials functions of the mean angle of attack as:

$$\begin{aligned} \dot{\boldsymbol{x}}(t) &= [\boldsymbol{A_2\alpha(t)^2} + \boldsymbol{A_1\alpha(t)} + \boldsymbol{A_0}]\boldsymbol{x}(t) + [\boldsymbol{B}]C_{L_s}(\boldsymbol{\alpha}(t)) \\ \boldsymbol{C_L}_{\text{circulatory}}(t) &= [\boldsymbol{C_2\alpha(t)^2} + \boldsymbol{C_1\alpha(t)} + \boldsymbol{C_0}]\boldsymbol{x}(t) \end{aligned} \tag{12}$$

Note that the state space form results in the same $\boldsymbol{B}$ matrix. Figure 6 shows the variations of the coefficients of the transfer function (equivalently the state space model) with the operating angle of attack in the stall regime along with their quadratic fit. Two sets of data are excluded from this fit and kept for validation. These are the experimental data at $\alpha_0 = 25°, 40°$, respectively.

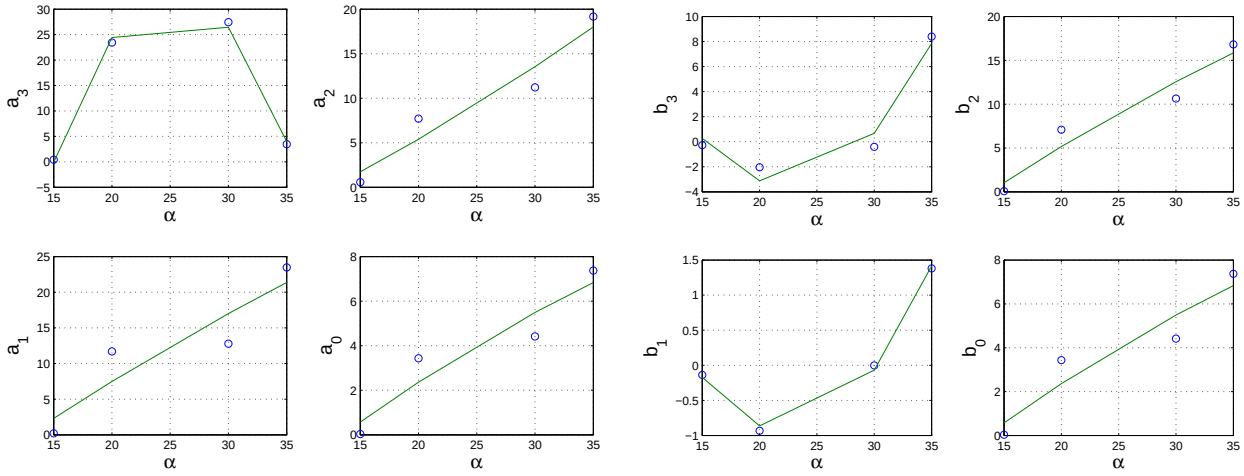

(a) Fourth order transfer function numerator coefficients

(b) Fourth order transfer function denominator coefficients

Figure 6. Variation of the transfer function coefficients with α_0 in the stall regime along with their quadratic fit.

VII. Results and Validation

The resulting model is then validated in frequency and time domains by comparing the model's prediction against the unsteady measurements for angles of attack $\alpha_0 = 25$ and 40 degrees.

A. Frequency domain comparison

Figure 7 shows the results for the proposed model and the experimental data with the fitted function based on the optimized coefficients. The plots in Fig.7 show that the proposed model captures the unsteadiness and the lift enhancement in the neighborhood of the amplitude jump associated with all the unsteady stall regime.

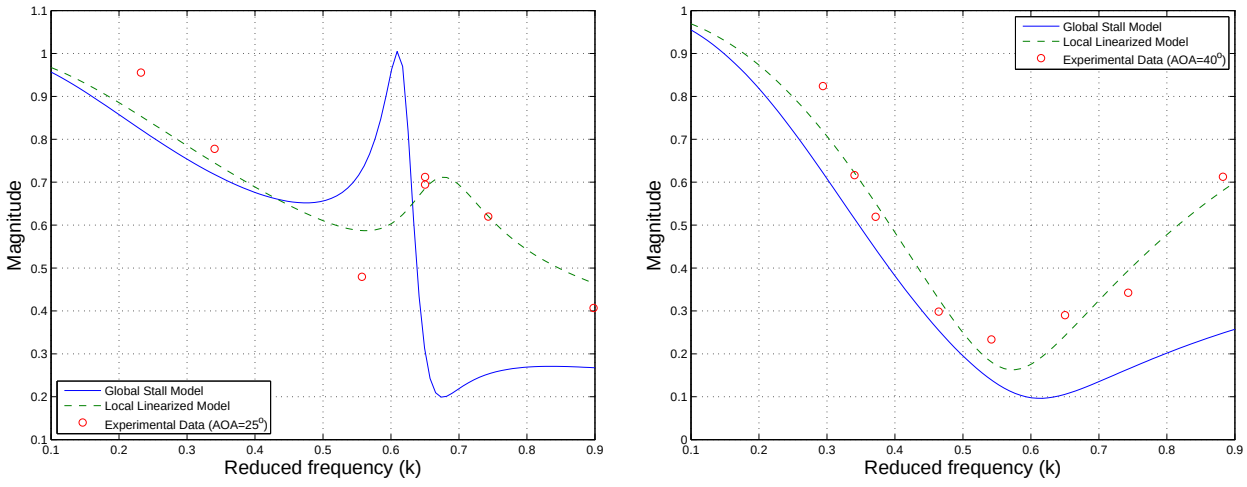

(a) Lift response function for test case $\alpha_o = 25^o$

(b) Lift response function for test case $\alpha_o = 40^o$

Figure 7. Global and Local models comparison with test cases

In fig.7(a), the model characterize an existing lift enhancement at k=0.61, this value corresponds to a maximum lift gain function of one. The model presented in 25^o test case shows an over-predicted trend than the local optimized model. Figure7(b) shows the global model also captured the dynamics at 40^o AOA test case with a slight discrepancy from the local optimized model.

B. Time domain Comparison

A more rigorous validation for the model presented in eq.12 is performed by comparing the time history of the obtained lift with the measured one. It should be noted that in this implementation, the effective angle of attack α_{eff} is used in the place of α in eq.12. Figures 8(a), 9(a), 10(a) and 11(a), show the time domain comparison between experimental data and the proposed global model at α_o=25^o and a wide range of reduced frequency (k=0.21, 0.35, 0.41 and 0.74), respectively. Figures 8(b), 9(b), 10(b) and 11(b), show time histories for the quasi-steady lift coefficient and the corresponding effective angle of attack.

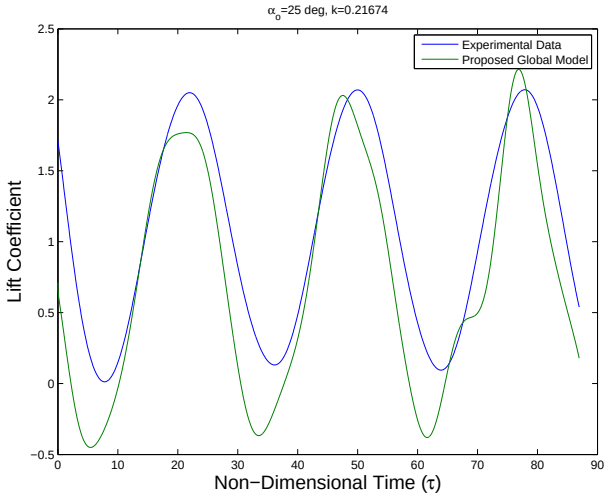

(a) Circulatory lift coefficient at 25^o AOA and k=0.21.

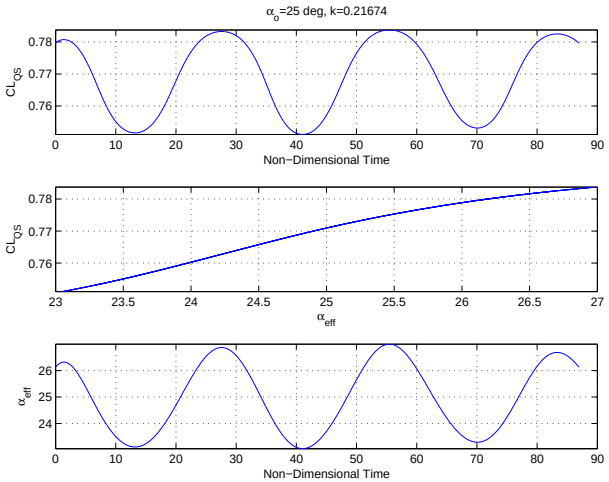

(b) Quasi-steady lift coefficient and α_{eff} at 25^o AOA and k=0.21.

Figure 8. Time domain comparison for $\alpha_0 = 25^o$ and k=0.21

Figure8 shows a good agreement with the experimental data with a slight shift appeared in the proposed model to be greater than the lift function amplitude of the experimental data. The quasi-steady lift coefficient shows a pure sinusoidal motion with time and linearly changes with the effective angle of attack. Increasing the reduced frequency in fig.9 and fig10, the proposed model shows satisfactory results for capturing the dynamics, while preserving the pure sinusoidal motion of the quasi-steady lift as well as the effective angle of attack. At a greater value of reduced frequency (k=0.74), we notice in fig.11 that the quasi-steady lift coefficient time history is no longer a pure sinusoidal. This is because this part of the $C_{L\alpha}$ curve characterized by a lack of monotonically nature (high non-linearity). Summing up the results, the proposed model shows acceptable results at low and high reduced frequency within the range of application.

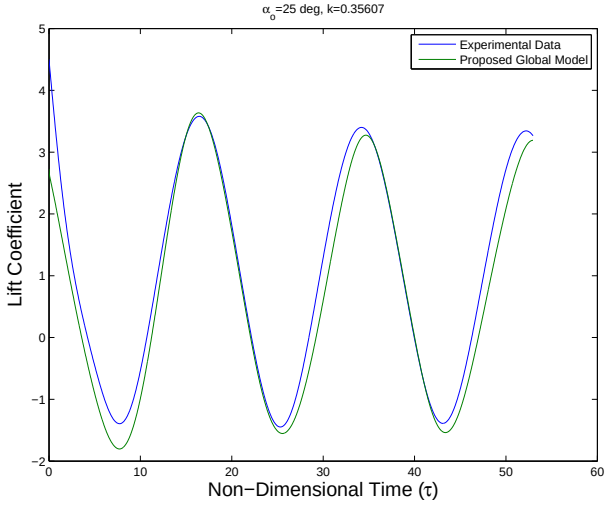

(a) Circulatory lift coefficient at 25^o AOA and k=0.35.

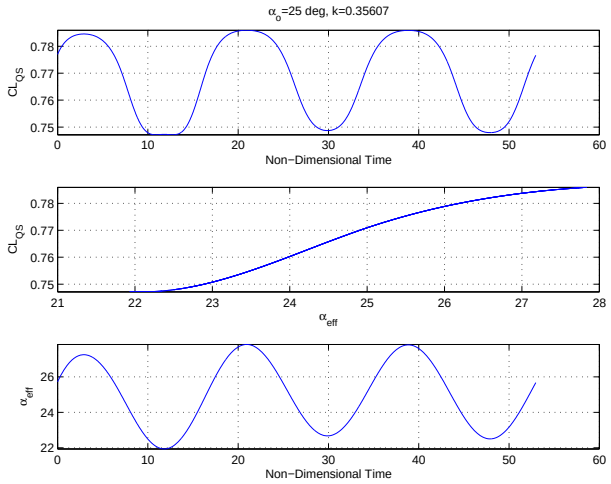

(b) Quasi-steady lift coefficient and α_{eff} at 25^o AOA and k=0.35.

Figure 9. Time domain comparison for $\alpha_0 = 25^o$ and k=0.35

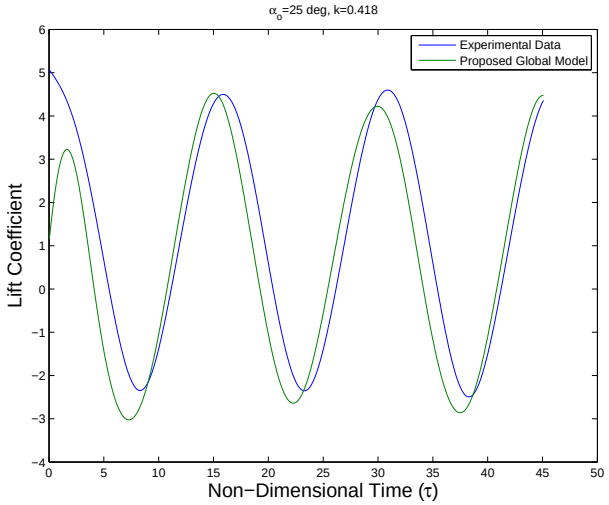

(a) Circulatory lift coefficient at 25^o AOA and k=0.41.

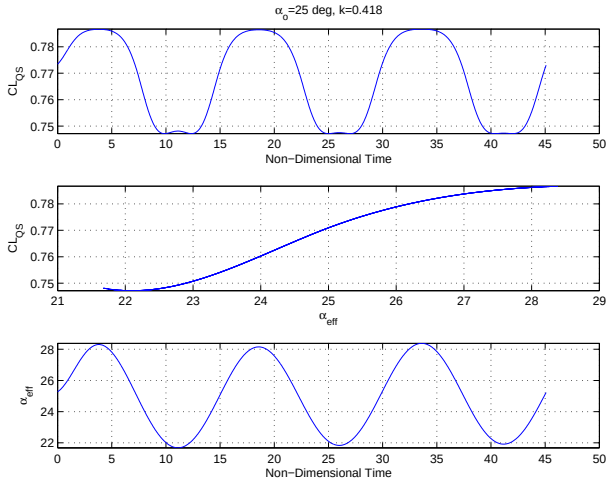

(b) Quasi-steady lift coeffiecint and α_{eff} at 25^o AOA and k=0.41.

Figure 10. Time domain comparison for $\alpha_0 = 25^o$ and k=0.41

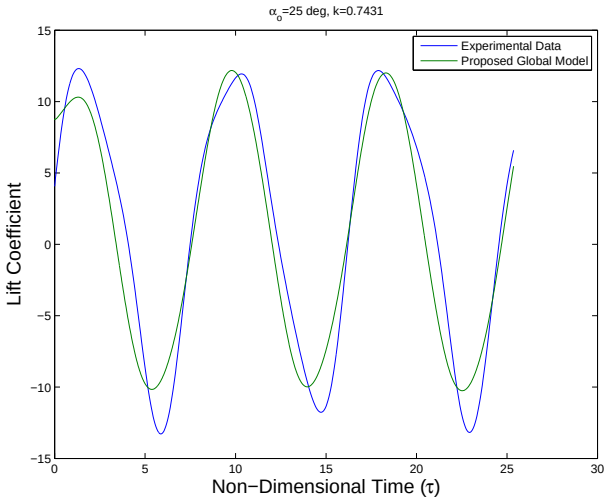

(a) Circulatory lift coefficient at 25^o AOA and k=0.74.

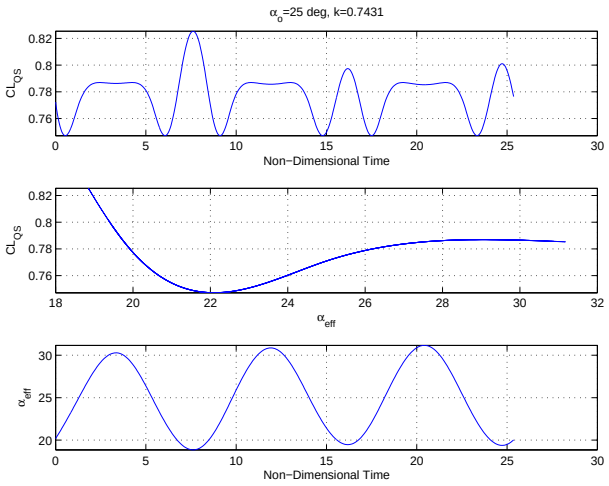

(b) Quasi-steady lift coeffiecint and α_{eff} at 25^o AOA and k=0.74.

Figure 11. Time domain comparison for $\alpha_0 = 25^o$ and k=0.74

VIII. Conclusion

In this work, a two-dimensional pure plunging experiment was performed at various frequencies and mean angles of attack. The frequency responses between the quasi-steady lift as an aerodynamic input and the unsteady circulatory lift component as an aerodynamic output are determined at different mean angles of attack up to 65°. An optimization-based fourth-order dynamical system model approximation is developed to match the obtained frequency responses at each mean angle of attack. These models are then written in a state space form. To combine the obtained models, the entries of the state space matrices are written as quadratic in the operating angle to attack. The developed model is then validated in the frequency and time domains against data set that were not included in the fitting process.

References

[1]Leishman, J. G. and Beddoes, T. S., "A Semi-Empirical Model for Dynamic Stall," *J. the American Helicopter Soc.*, Vol. 34, No. 3, 1989, pp. 3–17.

[2]Goman, M. and Khrabrov, A., "State-space representation of aerodynamic characteristics of an aircraft at high angles of attack," *Journal of Aircraft*, Vol. 31, No. 5, 1994, pp. 1109–1115.

[3]Reisenthel, P. H., "Development of a nonlinear indicial model for maneuvering fighter aircraft," *AIAA paper*, Vol. 896, 1996, pp. 1996.

[4]Brunton, S. L. and Rowley, C. W., "Empirical state-space representations for Theodorsens lift model," *Journal of Fluids and Structures*, Vol. 38, 2013, pp. 174–186.

[5]Theodorsen, T., "General Theory of Aerodynamic Instability and the Mechanism of Flutter," Tech. Rep. 496, NACA, 1935.

[6]Ansari, S. A., Zbikowski, R., and Knowles, K., "Non-linear Unsteady Aerodynamic Model for Insect-Like Flapping Wings in the Hover. Part1: Methodology and Analysis," *J. Aerospace Engineering*, Vol. 220, 2006, pp. 61–83.

[7]Ansari, S. A., Zbikowski, R., and Knowles, K., "Non-linear Unsteady Aerodynamic Model for Insect-Like Flapping Wings in the Hover. Part2: Implementation and Validation," *J. of Aerospace Engineering*, Vol. 220, 2006, pp. 169–186.

[8]Von Karman, T. and Sears, W. R., "Airfoil theory for nonuniformmotion." *J. Aeronautical Sciences*, Vol. 5, No. 10, 1938, pp. 379–390.

[9]Wang, C. and Eldredge, J. D., "Low-order phenomenological modeling of leading-edge vortex formation," *Theoretical and Computational Fluid Dynamics*, 2012, pp. 1–22.

[10]Taha, H. E. and Hajj, M. R., "State Space Representation of the Unsteady Aerodynamics of Flapping Flight," *Aerospace Science and Technology*, Vol. 34, 2014, pp. 1–11.

[11]Yan, Z., Taha, H. E., and Hajj, M. R., "Geometrically-exact unsteady model for airfoils undergoing large amplitude maneuvers," *Aerospace Science and Technology*, Vol. 39, 2014, pp. 293–306.

[12]Ramesh, K., Gopalarathnam, A., Granlund, K., Ol, M. V., and Edwards, J. R., "Discrete-vortex method with novel shedding criterion for unsteady aerofoil flows with intermittent leading-edge vortex shedding," *Journal of Fluid Mechanics*, Vol. 751, 2014, pp. 500–538.

[13]Rival, D. E., Kriegseis, J., Schaub, P., Widmann, A., and Tropea, C., "Characteristic length scales for vortex detachment on plunging profiles with varying leading-edge geometry," *Experiments in Fluids*, Vol. 55, No. 1, 2014, pp. 1–8.

[14]Triantafyllou, G., Triantafyllou, M., and Grosenbaugh, M., "Optimal thrust development in oscillating foils with application to fish propulsion," *Journal of Fluids and Structures*, Vol. 7, No. 2, 1993, pp. 205–224.

[15]Anderson, J., Streitlien, K., Barrett, D., and Triantafyllou, M., "Oscillating foils of high propulsive efficiency," *Journal of Fluid Mechanics*, Vol. 360, No. 1, 1998, pp. 41–72.

[16]Ohmi, K., Coutanceau, M., Daube, O., and Loc, T. P., "Further experiments on vortex formation around an oscillating and translating airfoil at large incidences," *Journal of Fluid Mechanics*, Vol. 225, 1991, pp. 607–630.

[17]Wang, Z. J., "Dissecting insect flight," *Annu. Rev. Fluid Mech.*, Vol. 37, 2005, pp. 183–210.

[18]Choi, J., Colonius, T., and Williams, D. R., "Surging and plunging oscillations of an airfoil at low Reynolds number," *Journal of Fluid Mechanics*, Vol. 763, 1 2015, pp. 237–253.

[19]Cleaver, D. J., Wang, Z., and Gursul, I., "Bifurcating flows of plunging aerofoils at high Strouhal numbers," *Journal of Fluid Mechanics*, Vol. 708, 2012, pp. 349–376.

[20]Panah, A. E. and Buchholz, J. H., "Parameter dependence of vortex interactions on a two-dimensional plunging plate," *Experiments in Fluids*, Vol. 55, No. 3, 2014, pp. 1–19.

[21]Oppenheim, A. V., Schafer, R. W., Buck, J. R., et al., *Discrete-time signal processing*, Vol. 2, Prentice-hall Englewood Cliffs, 1989.

[22]Zakaria, M. Y., Taha, H. E., and Hajj, M. R., "Experimental Investigations of the Lift Frequency Response at High Angles of Attack," , No. 1503, January 2015, pp. 18.

[23]Jones, R. T., "Operational treatment of the nonuniform lift theory to airplane dynamics," Tech. Rep. 667, NACA, 1938.

[24]Peters, D. A., "Two-dimensional incompressible unsteady airfoil theoryAn overview," *J. Fluids and Structures*, Vol. 24, 2008, pp. 295312.

[25]Jefferys, E., Broome, D., and Patel, M., "A transfer function method of modeling systems with frequency-dependent coefficients," *Journal of Guidance, Control, and Dynamics*, Vol. 7, No. 4, 1984, pp. 490–494.

[26]Wang, Z., "Vortex shedding and frequency selection in flapping flight," *Journal of Fluid Mechanics*, Vol. 410, 2000, pp. 323–341.